Frequency dependence of sound propagation in superfluid-filled porous media

Kevin Warner*
Department of Physics and Astronomy, University of Delaware, Newark, Delaware 19716

J. R. Beamish
Department of Physics, University of Alberta, Edmonton, Alberta, Canada T6G 2J1
(Received 21 March 1994; revised manuscript received 22 July 1994)

We have studied the acoustics of fluid-filled porous media by measuring the velocity and attenuation of ultrasonic (4 to 31 MHz) shear waves in several different ceramic materials. We used liquid helium as the pore fluid and made measurements down to low temperatures where the helium was superfluid. This allowed us to completely eliminate the effects of viscosity and thus to unambiguously determine the velocity changes and attenuation due to the Biot mechanism (fluid "sloshing" in the pores). By using ceramics with different pore sizes and a corresponding wide range of permeabilities (from 2.6×10^{-14} to 3.5×10^{-11} cm^2) we were able to make measurements in both the low-frequency regime (where the fluid is viscously locked to the porous frame) and in the high-frequency regime (where most of the fluid is decoupled from the frame). One of the samples had an extremely high porosity (92%), allowing us to study the fluid motion in a very open geometry. In all cases, we found that the Biot model could quantitatively describe the temperature and frequency dependence of our results. This allowed us to determine the structural parameters of the porous media (pore tortuosity c, permeability κ_a and effective pore size Λ), something which has previously required measurements of the Biot slow wave (fourth sound and second sound in superfluid helium). The acoustically determined parameters were compared to the independently measured static permeability, κ_0, and to previous experimental and theoretical work on model porous media. Our results indicate that, even in materials with irregular pores and a range of length scales, acoustic measurements made in either the low- or high-frequency regime can be used to estimate the permeability.

INTRODUCTION

Fluid-filled porous media have been intensively studied using a wide variety of experimental and theoretical techniques. This is not only because of their technological importance, but also because they provide opportunities to examine the effects of complex, disordered pore structures on the properties of the fluids confined in the pores. In applications such as seismology, an important goal is to extract information about structural properties such as permeability. However, there are many possible sources of attenuation in such systems,[1-4] for example, friction between grains, viscous shear or "squirt" of fluid in narrow cracks, flow between regions of partial saturation, as well as the "sloshing" of fluid in pores considered by Biot.[5] Although the irregular structure of most porous media makes it difficult to relate the sound velocity and attenuation directly to pore microstructure, considerable progress has been made recently by identifying a few geometric parameters which can, in principle, be determined from acoustic measurements. Experimentally, however, only synthetic porous media such as water-saturated glass bead samples have been studied in detail. It would be very useful to see whether quantities like permeability can be predicted from acoustic measurements in materials with complex pore structures and a broad distribution of pore sizes.

The motion of a fluid in a porous medium during transport or acoustic measurements is controlled by the pore geometry and the fluid's properties. The fluid's effect on the propagation of a sound wave depends on whether the fluid moves relative to the solid matrix. This in turn depends on the "viscous penetration depth" δ_{visc}, the thickness of the fluid layer dragged into motion by an oscillating pore surface. At low sound frequencies, this is much larger than the pore size. The fluid is then viscously locked to the solid and its main effect is to increase the porous medium's effective density. The sound attenuation is due to the remaining fluid motion, which is controlled by the static permeability κ_0. At high frequencies, however, only a thin surface layer is dragged along with the solid. The effective density is then smaller and the sound wave is strongly attenuated by viscous dissipation in the surface layer. In order to use acoustic measurements as a probe of pore microstructure, we would therefore like to vary the viscous penetration depth over as wide a range as possible, from smaller to larger than the pore sizes of interest. The obvious way to do this is to make measurements over a range of sound frequencies, but we can also change the properties of the fluid. Using liquid helium as a pore fluid has unique advantages for such experiments. The existence of a superfluid phase means that the limit of zero viscosity can be achieved simply by reducing the temperature. This allows viscous effects to be unambiguously separated from those due to other mechanisms such as scattering by pores. Also, both the density and the viscosity of helium can be continuously varied, either by changing the temperature or

by applying modest pressures. Johnson and co-workers[6] have shown how the acoustic modes in superfluid helium (fourth sound and second sound) can be used to characterize the geometry of simple porous media. However, the more conventional fast longitudinal and transverse modes have not yet been exploited for this purpose, even though they can provide essentially the same information.

We earlier reported measurements of the attenuation of ultrasonic shear waves in a helium-filled ceramic sample.[7] These did not appear to agree with the predictions of Biot's theory[5] of the acoustics of fluid-filled porous media. However, Gist[8] has pointed out that, if the effective pore size was considerably smaller than we estimated, our results might still be consistent with Biot's theory. To test this possibility, and to determine the extent to which acoustic measurements with fast modes (shear or longitudinal) can be used to determine the structure and properties of porous media, we have measured the velocity and attenuation of ultrasonic waves in a number of helium-filled materials. By varying the temperature and sound frequency and by using materials with a range of pore sizes, we have been able to make measurements in both the low- and high-frequency regimes. In this paper, we present our results and make quantitative comparisons to theoretical predictions. We discuss the applicability of Biot's theory, which is based on models of pores as smooth, geometrically simple channels, to complex materials with a distribution of pore sizes.

BACKGROUND

The theoretical framework for describing sound propagation in fluid-filled porous media is provided by the work of Biot.[5] By treating the motion of the solid matrix and of the fluid on an equal footing, Biot derived equations for sound propagation which included the effects of relative motion between the fluid and the pore matrix. The importance of this "sloshing" depends on the viscous penetration depth which, for an oscillation of angular frequency ω, is given by

$$\delta_{\text{visc}}=\left[\frac{2\eta}{\rho_f\omega}\right]^{1/2}, \tag{1}$$

where ρ_f is the fluid's density and η is its viscosity. For a pore of radius R, this defines a critical frequency

$$\omega_c=\frac{2\eta}{\rho_f R^2} \tag{2}$$

at which $\delta_{\text{visc}}=R$. At frequencies well below ω_c, the penetration depth is larger than the pore size and essentially all the fluid moves with the frame. Above ω_c, on the other hand, δ_{visc} is smaller than the pore size and much of the fluid can decouple from the solid, with corresponding changes in the sound velocity and attenuation.

Biot considered two simple models of a porous medium, one of uniform cylindrical pores (radius R) and another of two-dimensional ductlike pores (thickness $2R$). He found that the frequency dependence of the fluid motion was almost identical in the two cases, provided the frequency was appropriately rescaled. He therefore proposed that a simple model, such as that of cylindrical pores, should describe the behavior in a more general porous medium. The porous medium would then be characterized by four geometrical parameters which could be taken as the porosity ϕ, the tortuosity c, the static permeability κ_0, and an effective pore size which determines the crossover from high- to low-frequency behavior. The porosity ϕ is the volume fraction occupied by the pores ($0<\phi<1$). The tortuosity c is related to the "formation factor" which appears in measurements of the electrical conductivity of a sample whose pores contain a conducting fluid. It can vary from unity (for straight pores parallel to the motion) to infinity (for isolated pores or pores perpendicular to the motion). The permeability κ_0 relates the fluid flow to the pressure gradient in a dc flow experiment. It is given, for example, by $\kappa_0=\phi R^2/8c$ for nonintersecting cylindrical pores.

In discussing Biot's theory, we will concentrate on the case of transverse waves, since these were used in all of the experiments described in this paper. The behavior of longitudinal waves is qualitatively the same. For a shear wave of frequency ω, Biot's equations give for the wave vector k

$$k^2=\frac{\omega^2}{v_0^2}\left[1-i\frac{\rho_f^2\omega}{\rho_T\eta}\kappa(\omega)\right]. \tag{3}$$

In this formula, ρ_T is the system's total density and v_0 is the transverse velocity in the limit of low frequency. The velocity and attenuation of the shear wave are found from the real and imaginary parts of k as

$$v=\frac{\omega}{|\text{Re}(k)|} \tag{4}$$

and

$$\alpha=\text{Im}(k)\,. \tag{5}$$

The "dynamic permeability" $\kappa(\omega)$ in Eq. (3) is given by

$$\kappa(\omega)=\frac{\kappa_0}{F(\omega)-ic\omega\rho_f\kappa_0/\eta\phi}, \tag{6}$$

where $F(\omega)$ describes the deviation from Poiseuille flow at finite frequencies. For simple pore geometries it can be calculated exactly. For example, for uniform cylindrical pores it is given by

$$F(\omega)=\frac{\sqrt{-ix}}{4}\frac{J_1(\sqrt{-ix})}{J_2(\sqrt{-ix})}, \tag{7}$$

where the argument x which appears in the Bessel functions is

$$x=\frac{\rho_f\omega R^2}{\eta}=\frac{2\omega}{\omega_c}\,. \tag{8}$$

At low frequencies ($\omega\ll\omega_c$) where the flow is Poiseuille, $F(\omega)=1$ and $\kappa(\omega)=\kappa_0$. At high frequencies ($\omega\gg\omega_c$), on the other hand,

$$\kappa(\omega)\approx i\frac{\eta\phi}{c\rho_f\omega}\left[1-i\frac{\delta_{\text{visc}}}{R}\right] . \tag{9}$$

Although in any porous medium $\kappa(\omega)$ must approach the static permeability κ_0 at sufficiently low frequency, one might expect that a material with irregular pores or a wide range of pore sizes would have a frequency dependence rather different from the uniform cylindrical pore expression (7). However, Johnson and co-workers[9,10] have shown quite generally that the high-frequency limit of $\kappa(\omega)$ is of the form

$$\kappa(\omega)\approx i\frac{\eta\phi}{c\rho_f\omega}\left[1-i\frac{\delta_{\text{visc}}}{\Lambda}\right] , \tag{10}$$

where the length scale Λ is an effective size for *dynamically connected* pores. It is a pore-volume-to-surface ratio weighted by $u(r)$, the local value of the fluid flow velocity at high frequencies. That is,

$$\frac{2}{\Lambda}=\frac{\int|u(r_W)|^2dA}{\int|u(r)|^2dV} , \tag{11}$$

where the integration in the numerator is over the pore walls while that of the denominator is over the pore volume. From Eqs. (9) and (10), we see that Λ is just the pore radius R for cylindrical pores. Johnson, Koplik, and Dashen[10] pointed out that a simple interpolation between the low- and high-frequency behavior, for example, the function

$$F(\omega)=\left[1-i\frac{4c^2\kappa_0^2\rho_f\omega}{\eta\Lambda^2\phi^2}\right]^{1/2} , \tag{12}$$

provides a good approximation to $F(\omega)$, even in models with a rather broad distribution of pore radii.

We now consider the sound velocity and attenuation. At low frequencies, the fluid and frame move together and so act as a single medium with a total density

$$\rho_T=\rho_p+\phi\rho_f , \tag{13}$$

where ρ_p is the density of the empty porous material. Two sound modes then propagate, the usual transverse and longitudinal ones. Since the fluid does not contribute to the system's shear modulus, the velocity of the transverse wave is given by

$$v_0=\left[\frac{\mu_p}{\rho_T}\right]^{1/2}=\left[\frac{\mu_p}{\rho_p+\phi\rho_f}\right]^{1/2} , \tag{14}$$

where μ_p is the shear modulus of the empty porous frame. The corresponding expression for the velocity of the longitudinal mode is more complicated since the fluid does contribute to the bulk modulus of the system as well as to the density. In this low-frequency regime, any decrease in the viscous penetration depth (e.g., by increasing the frequency) results in more motion of the fluid in the pores and larger attenuation. The low-frequency attenuation of a transverse wave is then

$$\alpha=\frac{\kappa_0\rho_f^2\omega^2}{2\rho_T v_0\eta} . \tag{15}$$

At high frequency (or, equivalently, for small viscosity or large pores), only fluid within the viscous penetration depth is locked to the pore surface. This allows a third mode to propagate, the "Biot slow wave," in which the fluid moves relative to the porous frame. The decoupling of the fluid also affects the other sound modes since, for example, it reduces the effective density and thus increases the velocity of transverse waves, giving the high-frequency limit

$$v_\infty=\left[\frac{\mu_p}{\rho_T-\phi\rho_f/c}\right]^{1/2} . \tag{16}$$

The effective density is not just that of the porous frame because, even if the viscosity is zero, the tortuosity only allows a fraction $1/c$ of the fluid to decouple (and the rest remains inertially entrained). The corresponding high-frequency attenuation is

$$\alpha=\frac{\phi}{c\rho_T v_0}\frac{1}{\sqrt{1-\phi\rho_f/c\rho_T}}\frac{\sqrt{\eta\rho_f\omega}}{\Lambda} , \tag{17}$$

which reflects the fact that the dissipation is all occurring in a thin layer on the pore surface (whose area is proportional to $1/\Lambda$).

The above discussion indicates that it should be possible to characterize the geometry of a porous medium using measurements of sound velocity and attenuation. The porosity ϕ can be determined from the change in the low-frequency sound velocity when the pores are filled with a fluid of known density, while the tortuosity c can be found from the corresponding velocity change at high frequency. The permeability κ_0 and the pore-size parameter Λ can be determined from the attenuation in the low- and high-frequency limits or, alternatively, from the frequency dependence of the velocity in the crossover region.

The combination of parameters $M=8c\kappa_0/\phi\Lambda^2$ which relates the low- to the high-frequency behavior is equal to 1 for cylindrical pores. Numerical calculations by Johnson and co-workers[9,10] showed that it was also close to 1 for models with a fairly wide range of pore sizes. They speculated that this relationship between Λ and κ_0 might be valid more generally, raising the possibility of estimating permeabilities from high-frequency acoustic measurements alone. Zhou and Zheng[11] have calculated the dynamic permeability for a number of more realistic models with variable width pores. They found that, as long as the narrow "throats" between pores were not too sharp, the complete frequency dependence of $\kappa(\omega)$ for all the models could be approximately collapsed onto a single curve using only two scaling parameters (which they took to be the static permeability κ_0 and a characteristic frequency $\omega_0=\eta\phi/\rho_f\kappa_0 c$). Chapman and Higdon[12] have recently made detailed calculations for a model consisting of periodic lattices of spheres. They found that the quantity M varied somewhat with porosity, from close to 1 for low porosities to greater than 2 at intermediate porosi-

ties. In their models M approached zero as the porosity approached 1. Several other authors[13–15] have recently discussed how pore roughness, pore-size dispersion, and sharp orifices affect the relationship between Λ and κ_0.

Measurements on water-filled samples of glass beads, crushed glass, and sand[6,16,17] have confirmed this "universal" behavior of the dynamic permeability and found that M was indeed close to 1. The form of the scaled permeability found in both the models and the experiments was consistent with the Biot form and with the simpler function[18] (12). The apparently universal behavior of $\kappa(\omega)$ appears to limit the amount of information on pore-size distributions that can be extracted from acoustic measurements. However, M was significantly different from 1 and scaling did not hold in models with knifelike throats and when the porosity was close to 1. Other authors[19,20] have also modified the Biot model to account for more complicated pore geometries. In porous materials with a wide range of pore sizes we would also expect the crossover between low- and high-frequency acoustic behavior to be broader than predicted by Biot.

An extreme example in which different length scales are crucial is that of fractal structures, which have been proposed for a number of materials, from sedimentary rocks to silica aerogels. For a fractal surface the effective area depends on the length L of the "yardstick" used to make the measurement, varying as

$$S \propto L^{2-d} , \tag{18}$$

where d is the fractal dimension of the surface ($d=2$ for smooth surfaces). In acoustic measurements, the penetration depth $\delta_{\rm visc}$ provides a yardstick which can be varied, for example, by changing the sound frequency. The fractal dimension of the pore surface might then be related to the frequency dependence of the sound attenuation. The simplest possibility, as proposed by Johnson, Koplik, and Dashen,[10] is to replace the $1/\Lambda$ dependence of the attenuation in expression (17) by a fractal surface area proportional to $\delta_{\rm visc}^{2-d}$. This would change the $(\eta\rho_f\omega)^{1/2}$ behavior of the high-frequency attenuation to the form

$$\alpha \propto \eta^{(3-d)/2}\rho_f^{(d-1)/2}\omega^{(d-1)/2} . \tag{19}$$

Recently, a more detailed calculation by Koch[21] showed that the frequency dependence of the attenuation need not reflect the true fractal dimension of the pore surface. However, in his model the smaller pores were all dead ends in which there was very little relative motion of the fluid. If all pores are connected to allow flow, the smaller pores will make a larger contribution to the attenuation.

Although the Biot theory dates to the 1950s, it was not until relatively recently that its wide applicability was demonstrated experimentally. The most dramatic confirmation was the observation[22] of the slow wave in glass bead samples filled with water. Attempts to detect this mode in water-saturated rocks and similar materials have not been very successful, but Johnson has pointed out[23] that the well-known "fourth-sound" mode of superfluid helium in pores is precisely the Biot slow wave. He also noted[24] the substantial advantages of using superfluid helium as the pore fluid in acoustic measurements. Helium is very compressible so its density, bulk modulus, and viscosity can be changed considerably by applying modest pressure.[25] Even more valuable is the possibility of further varying or even totally eliminating the effects of viscosity by cooling below the λ transition at $T_\lambda = 2.17$ K. Helium then becomes a superfluid and behaves as a mixture of a normal (viscous) component with density ρ_n, viscosity η, and a superfluid (zero-viscosity) component with density ρ_s. Figure 1 shows the temperature dependence of ρ_n, ρ_s, and η. The fraction of the fluid in the normal component varies from essentially zero below 1 K to 100% at and above T_λ, allowing one to vary the viscous penetration depth over a considerable range. However, the concept of viscosity must be used with care at the lowest temperatures. The normal-fluid component can be regarded as a gas of phonons and rotons and the rapid rise in its viscosity below 1.2 K is due to their mean free paths becoming large. If the mean free paths become larger than either the viscous penetration depth $\delta_{\rm visc}$ or the pore size R, then the hydrodynamic description breaks down and the effect of the fluid should be described in terms of scattering of phonons and rotons from the pore walls. Measurements of the transverse acoustic impedance of superfluid helium[26] have shown that, for a frequency of 34 MHz, the hydrodynamic description breaks down below 1.4 K, so comparisons to the Biot model should be made at higher temperatures.

Note that a superfluid-filled porous medium is really a three-component system since ρ_n and ρ_s can move independently of one another. The superfluid fraction, having zero viscosity, is always in the high-frequency limit, while the normal-fluid fraction may be in either the low-

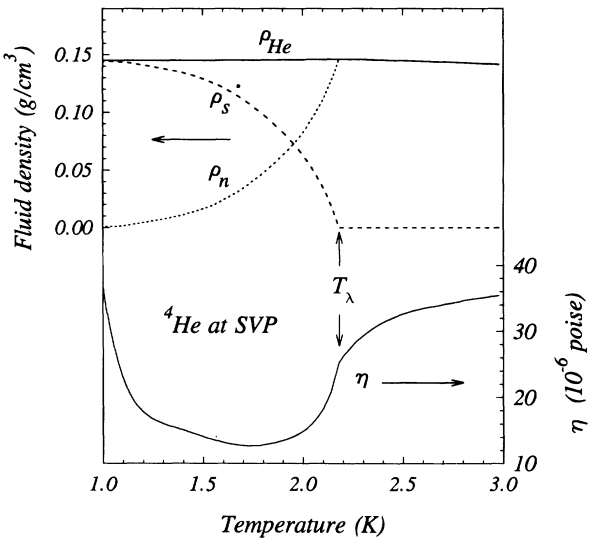

FIG. 1. Properties of liquid helium at its saturated vapor pressure (SVP). The upper curves (and left axis) are the density of the normal-fluid fraction, ρ_n (dotted line), the superfluid fraction, ρ_s (dashed line), and the total-liquid density $\rho_{\rm He}$ (solid line). The lower curve (right axis) is the fluid's viscosity. Below the superfluid transition ($T_\lambda = 2.176$ K), the viscosity is that of the normal-fluid fraction.

or high-frequency limit, depending on the temperature as well as on the pore size and sound frequency. Johnson and co-workers[6] have shown that measurements of the damping of the slow waves (fourth sound and "second sound," a temperature wave which also propagates in superfluid helium) agree well with theoretical expectations and can be used to determine the pore-size parameter Λ, although the materials studied had rather simple structures (sintered glass beads[27] or bronze spheres[28]). The transverse and fast longitudinal modes in fluid-filled porous media have so far provided less information on pore microstructure even though they are more accessible with conventional techniques and are important in practical applications. This is partly because in laboratory measurements the Biot contribution to the attenuation is usually small and difficult to separate from that due to other mechanisms, such as scattering by pores or dissipation from fluid "squirting" from cracks. Attenuation with the expected high-frequency $\omega^{1/2}/R$ behavior has been observed (after scattering losses have been subtracted) for longitudinal waves in unconsolidated, water-saturated glass beads[29] and for water-saturated sands.[30] Other relevant experiments have involved helium as the pore fluid. It is straightforward to incorporate the "two-fluid model" of superfluid helium into Biot's equations for the transverse and fast longitudinal modes. Because it has no viscosity, the superfluid fraction does not contribute to the attenuation and is always decoupled from the frame. Thus, as the temperature is lowered below T_λ and the superfluid fraction increases, the attenuation decreases and the velocity increases. Measurements at low frequency can be used to directly determine the superfluid fraction, since the transverse sound velocity then is just

$$v_0 = \left[\frac{\mu_p}{\rho_T - (\phi/c)\rho_s} \right]^{1/2} . \tag{20}$$

At high frequency, the normal fluid is also partially decoupled so the velocity increase when the helium becomes superfluid is smaller.

The two-fluid nature of superfluid helium may be incorporated into Biot's theory for the shear mode by replacing Eq. (3) with[8]

$$k^2 = \frac{\omega^2}{v_0^2} \left[1 - \frac{\phi}{c} \frac{\rho_s}{\rho_T} - i \frac{\rho_n^2 \omega}{\rho_T \eta} \kappa_n(\omega) \right] , \tag{21}$$

where $\kappa_n(\omega)$ is the dynamic permeability with the total-fluid density ρ_f replaced by the normal-fluid density ρ_n. This results from treating the normal and superfluid components as independent (and so does not describe the effects of sound-sound modes). By analogy with Eqs. (15) and (17), we then expect that the attenuation at low and high frequency will depend on the helium properties as ρ_n^2/η and $(\rho_n \eta)^{1/2}$, respectively. Figure 2 shows the temperature dependence of these combinations calculated from the data of Fig. 1.

Experiments with porous glasses such as Vycor and silica aerogel[31] clearly showed the expected increase in the transverse sound velocity when superfluid helium decoupled, demonstrating that such measurements can provide essentially the same information (pore tortuosity, superfluid density) as fourth-sound velocities. However, even at frequencies as high as 100 MHz, the Biot attenuation is too small to measure in materials with pores as small as those of Vycor (less than 100 Å in diameter). Two recent experiments have observed attenuation due to the Biot mechanism in materials with larger pores. Tingzhang, Iwasa, and Ikushima[32] made measurements of the attenuation of longitudinal ultrasonic waves in a superfluid-filled sample made from sintered silver powder. They were able to make measurements at only one frequency (5 MHz) but their data were consistent with the high-frequency $(\eta\rho_n)^{1/2}$ dependence of Eq. (19). However, little information about pore size or structure was available and an attenuation linearly dependent on ρ_n and independent of viscosity could describe the data equally well. In our measurements[7] on a porous ceramic sample we found that neither the dependence on frequency nor that on fluid viscosity agreed with the high-frequency prediction (17), even though the apparent pore sizes (about 1 μm) were much larger than the viscous penetration depth (about 0.02 μm at the highest frequency of 18 MHz). Instead, the attenuation appeared to increase linearly with both the frequency and the normal-fluid density, and was nearly independent of the viscosity. We interpreted these results as indicating that length scales much smaller than 1 μm were important, possibly due to surface roughness. In fact, our results were consistent with Eq. (19) for a surface fractal dimension close to 3, although the range of length scales probed in these experiments was much too small to conclude that the surface was actually fractal. As pointed out by Gist,[8] Biot's theory could still explain our results if the effective pore size was much smaller than 1 μm so that the frequencies used were in the crossover region.

To determine whether the Biot model can adequately describe the acoustic properties of materials with irregular pores, we have measured the velocity and attenuation

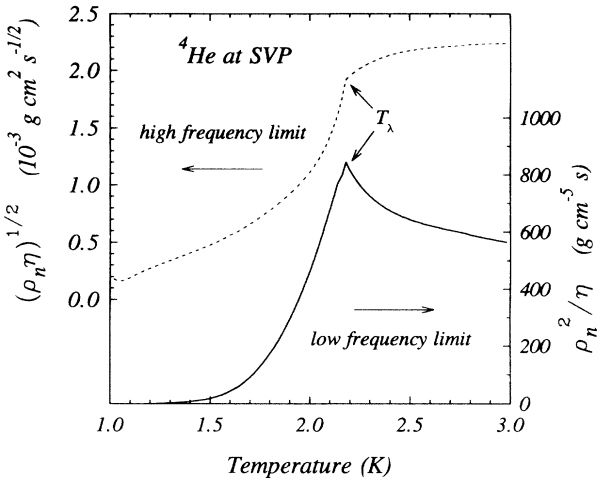

FIG. 2. The combinations of helium properties that enter the sound attenuation. The solid line (right axis) is the low-frequency combination ρ_n^2/η and the dashed line (left axis) is the high-frequency combination $(\rho_n\eta)^{1/2}$.

of transverse ultrasonic waves in three ceramic samples. The pore sizes varied from about 0.01 to 0.2 μm and the corresponding permeabilities varied by more than three orders of magnitude. With superfluid helium as the pore fluid and sound frequencies from about 4 to 30 MHz, we were able to study the behavior in the low- and high-frequency regimes, as well as in the crossover region. This allowed us to acoustically determine the permeability and the effective size of dynamically connected pores from the ultrasonic behavior of shear waves.

SAMPLE DESCRIPTION AND EXPERIMENTAL DETAILS

The porous materials used in this study were alumina (Al_2O_3) ceramics. They were characterized by a number of techniques, including measurements of porosity, permeability, and surface area. The sample density ρ_p and porosity ϕ were measured using the standard three-weight method (wet, dry, and buoyant). The static permeability κ_0 was found from the flow of water through a sample using a known pressure gradient. The specific surface area S was determined from nitrogen adsorption isotherms using the Brunauer-Emmett-Teller (BET) equation.[33] This information was used to determine an equivalent radius for cylindrical pores, $R_c = 2\phi/\rho_p S$. In addition, typical grain and pore sizes were estimated from scanning electron microscope (SEM) images. The tortuosity c was not independently measured. However, since the porosity and the density of liquid helium are known, the tortuosity can be directly determined from the difference between the transverse sound velocity when the pores were empty and the velocity after filling with helium (at low temperature where the normal-fluid fraction is negligible). That is,

$$c = \left\{ 1 - \frac{\rho_p}{\phi \rho_f} \left[\left[\frac{v(\text{empty})}{v(\text{full, low } T)} \right]^2 - 1 \right] \right\}^{-1} . \quad (22)$$

The first sample (identified as UCLA-0.01) was prepared[34] by slip-casting a very fine alumina powder (Linde A, nominal diameter 0.05 μm). Drying at 130 °C resulted in a material which could be machined to the desired shape. Because we did not sinter the green samples at elevated temperatures, the shear sound speed was quite low, 1.82×10^5 cm/s. The individual grains could not be resolved in SEM images but, from the measured porosity (52%) and specific surface area (59 m^2/g), the equivalent cylindrical radius is $R_c = 0.011$ μm. To measure the static permeability, we machined a cylinder (diameter 0.55 cm, height 0.19 cm) from the same piece that provided the ultrasonic sample. Epoxy was used to seal the outer surface and mount the sample on one end of a vacuum fitting, taking care not to get epoxy on the sample ends. Since the sample was quite fragile, a microscope was used to inspect it for cracks after the epoxy had hardened overnight. None were visible on the surface. One side of the sample was then connected to a graduated glass pipette and the other to a vacuum/pressure system. The whole system, including the sample, was evacuated to a pressure below 15 mTorr (to remove air from the pores) and then was saturated with degassed distilled water. The rate of water flow through the sample was then measured over a period of about 5 h, using two different pressure differentials across the sample (37 and 67 kPa). The resulting flow rates were 1.25×10^{-6} and 2.11×10^{-6} cm^3/s, respectively, giving nearly equal values for the permeability, 2.7×10^{-14} and 2.5×10^{-14} cm^2. In earlier measurements we had noticed that the small pores in this unsintered material caused it to swell and sometimes crack when saturated with water. With such small pores, even a small crack would result in an overestimate of the permeability. After the flow measurement was completed, we again examined it under the microscope (while still saturated with water), but did not find any cracks. Accordingly, we believe that the static permeability of our sample is $\kappa_0 = 2.6 \times 10^{-14}$ cm^2 with an uncertainty of about 10%.

The second sample[35] (du Pont–0.12) was prepared from considerably larger alumina powder (equivalent spherical diameter of 0.4 μm). As originally prepared, it was not mechanically strong enough to survive cooling and propagate sound waves at low temperatures, so we resintered it for 1 h at 1100 °C. This resulted in a shear sound speed of 2.70×10^5 cm/s, but no significant change in either the porosity (45%) or the surface area (3.5 m^2/g). These values correspond to an equivalent cylindrical radius $R_c = 0.12$ μm. The SEM images of fracture surfaces showed somewhat larger typical pores and grains, consistent with the nominal size of the starting powder and indicating that pore surfaces may be somewhat rough. The permeability was measured as 1.2×10^{-12} cm^2.

The last sample (GEL-0.16) was also alumina, but was made by a sol-gel process which allows homogeneous materials with very low densities to be prepared. Our sample had a porosity of 92% and a surface area of 35 m^2/g, giving $R_c = 0.16$ μm. The open structure meant that this material had an extremely low shear sound speed (8.12×10^4 cm/s) and a large permeability (3.6×10^{-11} cm^2). The properties of the three samples are summarized in Table I, which also includes parameters obtained by fitting the sound velocity and attenuation data below.

For the ultrasonic measurements, samples about 1 cm long were cut and their ends were polished flat and parallel. These were cleaned by boiling in a 30% hydrogen peroxide solution, rinsed in deionized water, and air dried. Lithium niobate transducers (41° X-cut shear, 20 MHz fundamental) were epoxied to both ends of a sample which was then sealed into a copper cell. This cell was mounted on a pumped ^{4}He cryostat which could be cooled to about 1.2 K. A capillary allowed us to flush the cell with high-purity helium gas and evacuate it several times before cooling. Temperatures were measured with an accuracy of about 5 mK (but a stability and resolution better than 0.1 mK) using calibrated germanium thermometers and a digital resistance bridge. The first sample (UCLA-0.01) was subsequently mounted on a dilution refrigerator so that measurements could be extended to lower temperatures.

The ultrasonic measurements were made using a phase-sensitive pulse-transmission technique. The output

TABLE I. Measured sample properties ($\phi, \rho_p, v, S, R_c, \kappa_0$), parameters determined by fitting acoustic data (c, κ_a, Λ), and the resulting value of the combination of structural parameters $M = 8c\kappa_0/\phi\Lambda^2$ discussed by Johnson, Koplik, and Dashen (Ref. 10).

Sample	ϕ	ρ_p (g/cm^3)	v (shear) (cm/s)	S (m^2/g)	R_c (cm)	κ_0 (cm^2)	c	κ_a (cm^2)	Λ (cm)	$M = 8c\kappa_0/\phi\Lambda^2$
UCLA-0.01	0.44[a]	1.64[a]	1.82×10^5	59	1.1×10^{-6}	2.6×10^{-14}	1.86	1.2×10^{-14}		
du Pont-0.12	0.45	2.20	2.70×10^5	3.5	1.2×10^{-5}	1.2×10^{-12}	1.48	7×10^{-12}	6.55×10^{-6}	0.74
GEL-0.16	0.92	0.335	8.21×10^4	35	1.6×10^{-5}	3.6×10^{-11}	1.20	6×10^{-11}	1.6×10^{-5}	1.47

[a]Values corrected for the effect of an "inert layer" of solid helium on the pore surfaces (see text).

of a signal generator was applied to a gated amplifier to generate rf pulses, about 2 μs long, of the desired frequency (from about 4 to 30 MHz). These were applied to one transducer and the resulting sound pulses were detected by the opposite transducer. Once the initial sound speed had been determined from the pulse transit time, changes in the velocity were calculated from the phase of the received signal. This was determined by splitting the signal pulse into two parts, one of which was compared directly to the output of the rf signal generator while the other was compared to a signal which had been phase shifted by 90°. The resulting in-phase and quadrature components of the signal could also be used to determine the amplitude of the received pulse. However, since slight imbalances between the two channels can give rise to spurious amplitude oscillations when the phase changes by large amounts, we also measured the pulse amplitude directly, before any phase detection took place, and used this to find the change in the attenuation.

The receiver used a heterodyne technique in which the phase detection and much of the amplification were done at a fixed intermediate frequency (155 MHz). The great advantage of this is that the ultrasonic frequency can be changed simply by adjusting the rf and local oscillator frequencies, without having to tune any other components. This allowed us to switch back and forth between different frequencies, under computer control and without any loss of resolution, so that measurements could be made over the entire frequency range during a single temperature sweep. With typical samples, our ultrasonic system could resolve velocity changes of a few parts per million and attenuation changes of 0.01 dB/cm and maintain this resolution over periods of several days. This stability was important since the system incorporated considerable signal averaging which meant that, for a typical duty cycle of 0.1%, as much as 15 min was required at each temperature to take data at all of the frequencies.

RESULTS AND DISCUSSION

We begin this section by presenting our results for the UCLA-0.01 sample. Its small pores should ensure that our ultrasonic measurements are in the low-frequency regime, making comparison to the Biot theory simple. We then show the comparable results for the other two samples, for which the measurements are in the high-frequency portion of the crossover regime.

In Fig. 3 we show the velocity of 11 MHz shear waves in our sample when the pores are empty (open symbols) and when they are filled with liquid helium at its saturated vapor pressure (closed symbols). The velocity in the empty sample is essentially constant in the temperature range shown (below 3 K). When the pores were filled, the velocity decreased (at 2.2 K) by about 2.3%. This is in good agreement with the predicted change due to the added density of the helium. The low-frequency expression (14) is expected to be valid since the crossover frequency is about 50 MHz (for pore radius $R = 11$ nm and helium above the superfluid transition). The slight increase in sound velocity between 2.2 and 3 K comes from the thermal expansion of the helium in the pores. The sudden increase at 2.138 K marks the onset of superfluidity and is due to the decoupling of the superfluid component ρ_s. However, not all of the helium is superfluid, even at the lowest temperatures. It is well known[36] that the first few atomic layers of helium on a solid surface are adsorbed as an "inert layer" which does not participate in superfluidity. In this sample, the large surface area means that about 6% of the helium in the pores is in the first monolayer, so the inert layer is significant. From measurements of the onset of superfluidity in thin films, we found that the inert layer coverage was 30 μmol/m^2 in this sample, similar to

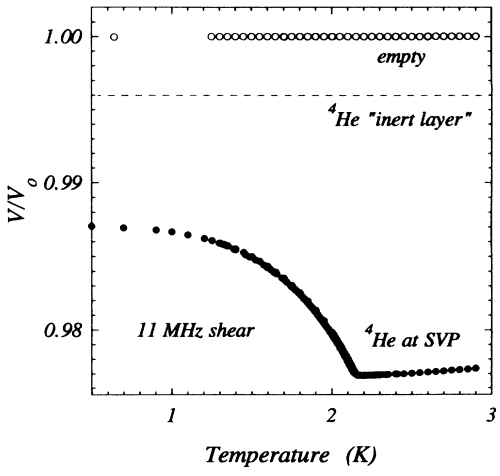

FIG. 3. The velocity of 11-MHz shear waves in the UCLA-0.01 ceramic sample, before and after filling the pores with liquid helium. The velocity v_0 in the empty sample is shown as open circles and is used to normalize the data. The solid circles are the data for filled pores. The dashed line is the experimentally determined sound speed when the solid "inert layer" of helium is adsorbed on the pore surfaces.

values found for other substrates. Since this helium is not fluid, it should be counted as part of the porous matrix. The sound speed with only the inert layer present is shown in Fig. 3 by the dashed line. The effective porosity is correspondingly reduced to 44% (from 53% in the empty sample). Since the porosity and the density of liquid helium are known, the tortuosity can be determined from the difference between the transverse sound velocity when only the inert layer is present and that when the pores are full (at low temperature where the normal-fluid fraction is negligible). That is,

$$c=\left[1-\frac{\rho_p}{\phi\rho_f}\left[\left[\frac{v(\text{inert})}{v(\text{full},\text{low } T)}\right]^2-1\right]\right]^{-1}, \qquad (23)$$

which gives $c=1.86\pm0.05$, consistent with the value measured in similar samples[34] using a fourth-sound technique.

Figure 4 gives the attenuation corresponding to the sound-velocity data of Fig. 3. In the empty sample (and with just the inert layer present), there is only a slight smooth increase in the attenuation up to 3 K. With helium filling the pores, the attenuation increases much more rapidly with temperature, reaching a peak at T_λ and then decreasing slightly. This is precisely the behavior expected in the low-frequency regime, as can be seen from Fig. 2. Since we appear to be in the low-frequency regime, as expected, the sound velocity should be independent of frequency. Figure 5 shows the measured sound velocity at frequencies of 4, 7, 11, and 18 MHz. The data at 7, 11, and 18 MHz have been offset vertically for clarity; without the offset all the curves fall essentially on top of the 4-MHz data, confirming that all the helium remains locked to the substrate up to at least 18 MHz. The solid line in Fig. 5 is just the low-frequency sound velocity, calculated from Eq. (20) using the porosity (44%), tortuosity (1.86), and the properties of bulk helium. It gives the correct behavior above the superfluid transition and at the lowest temperatures. However, the superfluid transition occurs at 2.138 K, compared to $T_\lambda=2.176$ in bulk helium, and the temperature dependence of the superfluid density ρ_s is modified near T_λ. These deviations from bulk behavior are due to the small pore size and have been seen in a variety of porous media.[37]

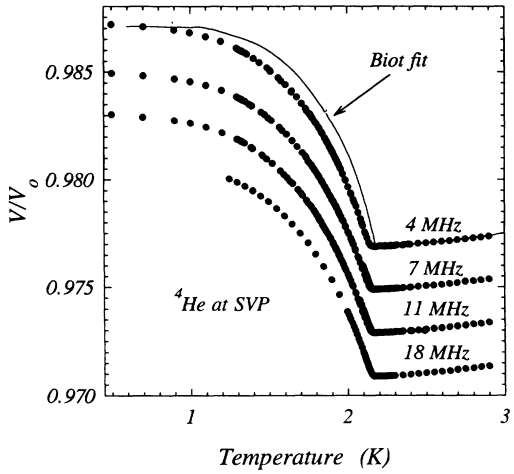

FIG. 5. The shear sound velocity in helium-filled UCLA-0.01 at different frequencies. The data at 7, 11, and 18 MHz have been offset vertically for clarity. The solid line is the calculated zero-frequency limit of the Biot model using the sample properties (ϕ,ρ_p,v_0) after correcting for the inert layer. The tortuosity was varied to match the sound speed at the lowest temperatures, giving $c=1.86$.

The corresponding attenuation is shown in Fig. 6, after subtracting the measured background attenuation in the empty sample. The data at all frequencies have the characteristic low-frequency decrease above T_λ, reflecting the η^{-1} dependence of the attenuation. The attenuation also increases rapidly with frequency, as expected. We compared the measured attenuation to the

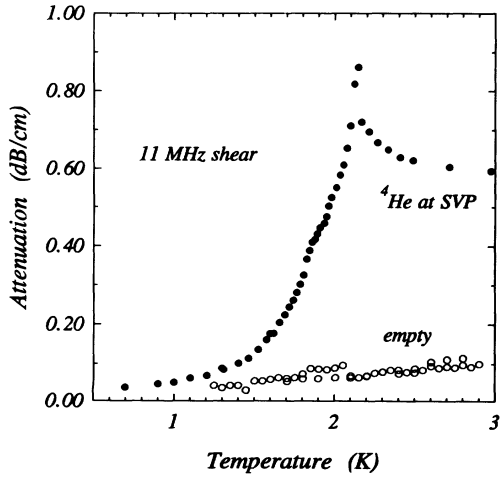

FIG. 4. The sound attenuation corresponding to the velocity data of Fig. 3. Open circles are for the empty sample, solid circles are for helium-filled pores.

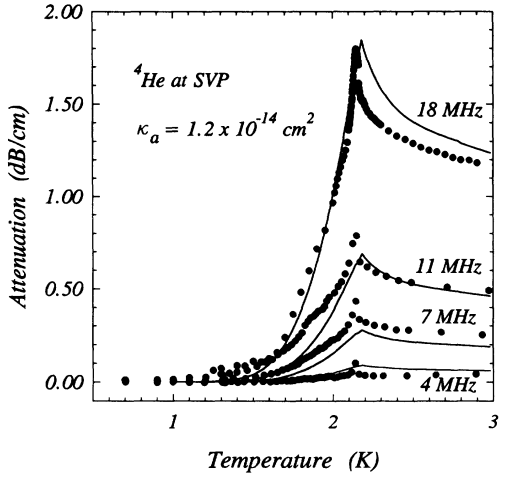

FIG. 6. The attenuation corresponding to the velocity data of Fig. 5. The small, smoothly varying background attenuation of the empty sample (see Fig. 4) has been subtracted at each frequency. The solid lines are the Biot fits with a permeability of $\kappa_a=1.2\times10^{-14}$ cm^2.

predictions of the Biot model with different values of the "acoustic" permeability κ_a and the pore-size parameter Λ. The solid lines show the best overall fit, obtained for $\kappa_a = 1.2 \times 10^{-14}$ cm^2. It is clear that the Biot mechanism is responsible for the attenuation and that we are in the low-frequency regime. In this regime, the attenuation is insensitive to the value of Λ and cannot be used to determine its value (the fits shown have $\Lambda = 10^{-6}$ cm). Both the frequency and temperature dependence are reasonably well reproduced by the fit. There are discrepancies at low frequencies, but the attenuation there is very small and subject to considerable experimental uncertainties.

The value of the permeability obtained from the fit is about half what we found in a static flow measurement. Berryman[38] has pointed out that inhomogeneities in the sample's permeability will affect κ_0 and κ_a differently, since flow experiments measure the global permeability while acoustic measurements probe the local permeability. However, he concluded that the permeability determined from the sound attenuation (κ_a) would be larger than that measured in a flow experiment (κ_0). We observe the opposite behavior, but inhomogeneities could still be important. For example, cracks in the sample would increase the flow permeability κ_0. At ultrasonic frequencies the fluid in the cracks would be in the high-frequency regime where its effect on the attenuation would be much smaller than would be expected based on the cracks' contribution to the permeability. Two other effects that may be significant are the swelling of the sample when saturated with water (which would result in an overestimate of κ_0) and the presence of the inert layer of helium on the pore surface which reduces the effective pore size by about 10%. Since the permeability varies as the cross-sectional area of the pores, we would expect the permeability with helium to be about 20% smaller than with water. Finally, in such small pores the density and viscosity of the helium may be different from their values in bulk helium.

Next, we show the results for the second sample, whose larger pores should put us in the crossover region. Figure 7 shows the velocity when the sample is empty and when it is filled with helium. In this sample the pores are large enough (equivalent cylindrical radius $R_c = 0.12$ μm) so that less than 1% of the helium atoms are on the surface and finite-size effects are not important. From the velocity change at low temperatures we find a tortuosity of 1.48 ± 0.1. From this and the porosity (45%) we can calculate the temperature dependence of the sound velocity in the low-frequency limit. The result, shown as a solid line, falls well below the measured velocities as the temperature is raised. It appears that only about half the normal-fluid fraction is coupled to the frame, indicating that a frequency of 4 MHz is somewhere in the middle of the crossover region. Figure 8 shows the corresponding attenuation. It is about an order of magnitude larger than that in the first sample, but has a similar temperature dependence. Figure 9 shows the frequency dependence of the velocity from 4 to 31 MHz. Since we are in the crossover region, as the frequency increases, less of the normal fluid moves with the matrix and the velocity increases. The corresponding attenuation, presented in

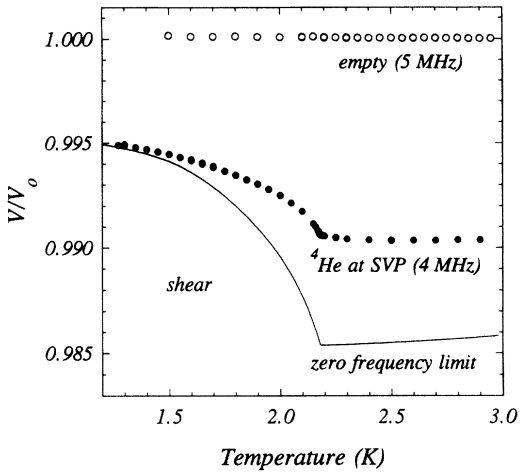

FIG. 7. Shear sound velocity before and after filling with helium (du Pont–0.12 sample). Open circles are v_0 for the empty sample (at 5 MHz) and solid circles are for the helium-filled sample (at 4 MHz). The line is the zero-frequency Biot calculation for a tortuosity $c = 1.48$. The faster sound speed measured above T_λ indicates that the normal fluid is partially decoupled from the porous frame.

Fig. 10, shows a crossover from the temperature dependence expected at low frequency (e.g., the 4-MHz data) to that expected at high frequency (e.g., the 31-MHz data). The solid lines in Figs. 9 and 10 are fits of the Biot model to the data using the parameters which give the best fit to the velocity data (the "acoustic" permeability $\kappa_a = 7 \times 10^{-12}$ cm^2 and the effective pore size $\Lambda = 6.55 \times 10^{-6}$ cm). The fits are very good, except for the attenuation at low frequencies, where the attenuation is smaller than predicted. The measured attenuation appears to be approaching the low-frequency regime faster than expected. However, if we adjust the parameters to improve the fit in this region, the fit to the velocity data deteriorates rapidly. In any case, the overall features of the data are reproduced very well by the Biot calculation.

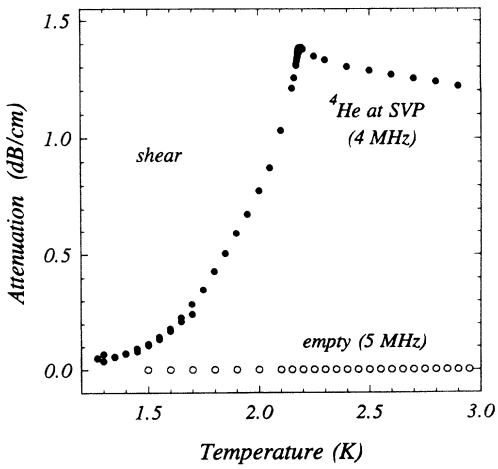

FIG. 8. The attenuation data (du Pont–0.12 sample) corresponding to Fig. 7.

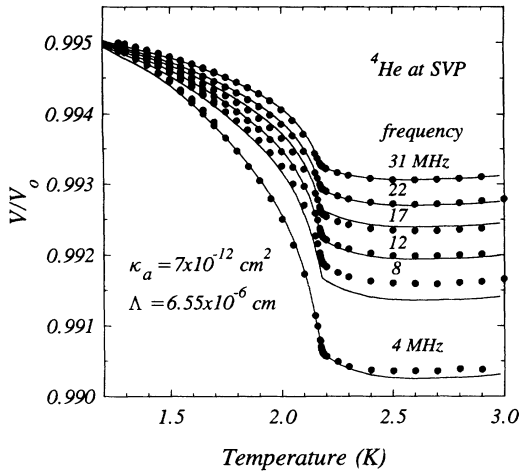

FIG. 9. The frequency dependence of the shear sound speed in the helium-filled sample (du Pont–0.12). The solid lines are the best fit to the Biot model (giving $\kappa_a = 7\times10^{-12}$ cm^2, $\Lambda = 6.55\times10^{-6}$ cm).

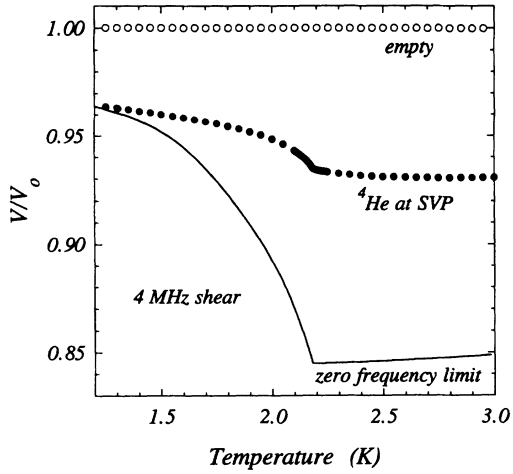

FIG. 11. Shear velocity at 4 MHz before and after filling with helium (GEL-0.16 sample). Open circles are v_0 for the empty sample and solid circles are for the helium-filled sample. The line is the zero-frequency Biot calculation for a tortuosity $c = 1.20$. The sound speed measured above T_λ indicates that most of the normal fluid is decoupled from the porous frame.

The value of the permeability extracted from the fit is higher than that measured in a flow experiment ($\kappa_0 = 1.2\times10^{-12}$ cm^2). However, the fits are not sensitive to the permeability, with $\kappa_a = 5\times10^{-12}$ cm^2 giving almost as good a fit, for example. On the other hand, the size parameter Λ cannot be varied by more than a few percent without giving a much poorer fit.

Finally, we show the results for the third sample, which has a much more open geometry (porosity 92%) which results in a small tortuosity (1.20 ± 0.05), as well as a large permeability ($\kappa_0 = 3.6\times10^{-11}$ cm^2). From Fig. 11 we can see that, even at 4 MHz, most of the normal fluid is decoupled so that we are further in the high-frequency regime than for the second sample. The 4-MHz attenuation, shown in Fig. 12, confirms this, since it has the characteristic high-frequency temperature dependence (compare to Fig. 2). Figures 13 and 14 show the frequency dependence of the velocity and attenuation from 4 to 12 MHz. The extremely high attenuation in this sample prevented measurements at high frequencies. The solid lines are the Biot fits with $\kappa_a = 6\times10^{-11}$ cm^2 and $\Lambda = 1.6\times10^{-5}$ cm. The fit is excellent. Again the fits are very sensitive to the value of Λ, but not to κ_0. If we use the independently measured value of the permeability, $\kappa_0 = 3.6\times10^{-11}$ cm^2, the fit is only slightly worse.

Given the parameters characterizing the three samples ($\phi, c, \kappa_0, \Lambda$), we can calculate the complete frequency dependence for the Biot model and show where our measurements fall with respect to the low- to high-frequency crossover. Figure 15 shows the frequency dependence of the attenuation and velocity calculated using the parameters from Table I and the properties of helium at 2.2 K,

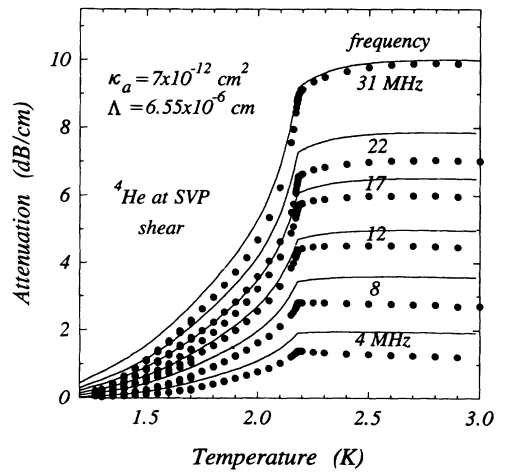

FIG. 10. The frequency dependence of the attenuation in the helium-filled sample (du Pont–0.12). The solid lines are the Biot predictions using the parameters determined from the velocity data (Fig. 9).

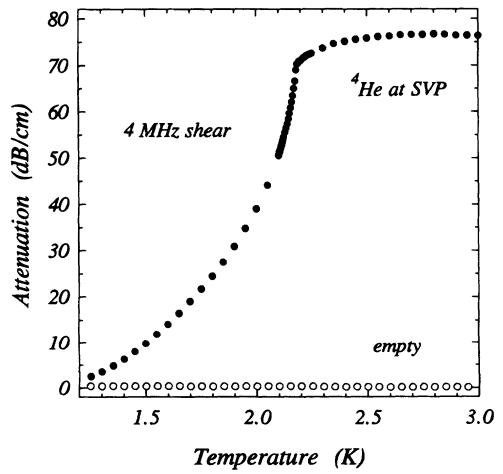

FIG. 12. The attenuation data (GEL-0.16 sample) corresponding to Fig. 11.

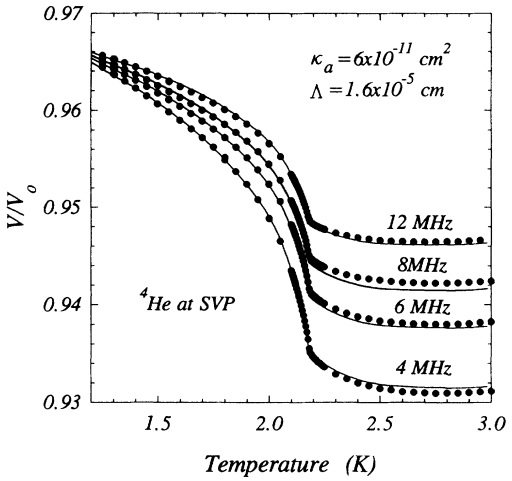

FIG. 13. The frequency dependence of the shear sound speed in the helium-filled sample (GEL-0.16). The solid lines are the best fit to the Biot model (giving $\kappa_a = 6\times10^{-11}$ cm^2, $\Lambda = 1.6\times10^{-5}$ cm).

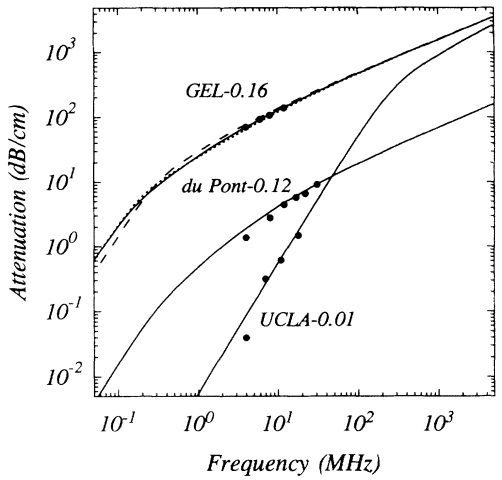

FIG. 15. The frequency crossover of the attenuation in the three samples. The symbols are the data at a temperature of 2.2 K (just above T_λ). The solid lines are the Biot predictions at the same temperature, calculated using the parameters from Table I. The dotted line for the GEL-0.16 sample (almost indistinguishable from the solid line) is a calculation using the same parameters but a simpler function for $F(\omega)$, as suggested by Johnson, Koplik, and Dashen (Ref. 10). The dashed line shows the effect of changing the permeability to 3.6×10^{-11} cm^2 in the Biot fit.

just above T_λ. The solid circles are the corresponding experimental data from Figs. 5–14. The crossover frequency appears as a knee separating the low-frequency behavior ($\alpha\sim\omega^2$) from that at high frequency ($\alpha\sim\omega^{1/2}$). We see that we are well on the low-frequency side of the crossover for the first sample (UCLA-0.01) but on the high-frequency side for the other samples (du Pont–0.12 and GEL-0.16). However, the crossover regions are so broad that, even in the GEL-0.16 sample, we have not reached the high-frequency limiting behavior. Over the frequency range of the measurements (4–12 MHz), both the measured and calculated attenuation vary approximately as $\omega^{0.6}$, rather than as $\omega^{1/2}$. For the second sample, du Pont–0.12, a similar power-law fit gives $\alpha\sim\omega^{0.9}$, midway between the low- and high-frequency limits. Figure 16 shows the corresponding frequency dependence of the sound velocity in the three samples. We have plotted the difference from the low-frequency sound speed $\Delta v(\omega) = v(\omega) - v(0)$, normalized by the total change from low to high frequency, $\Delta v(\infty) = v(\infty) - v(0)$. Again we see the difference between the UCLA-0.01 sample, which is in the low-frequency regime, and the others,

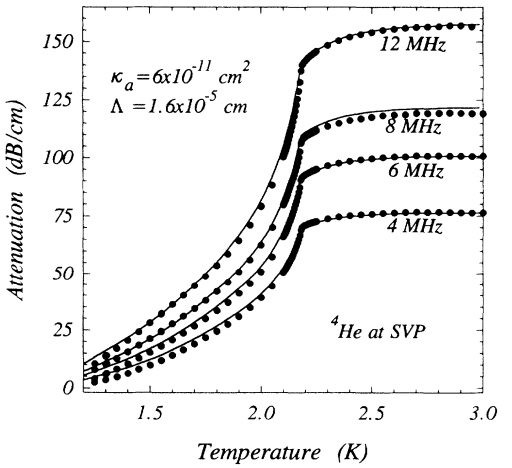

FIG. 14. The frequency dependence of the attenuation in the helium-filled sample (GEL-0.16). The solid lines are the Biot predictions using the parameters determined from the velocity data (Fig. 13).

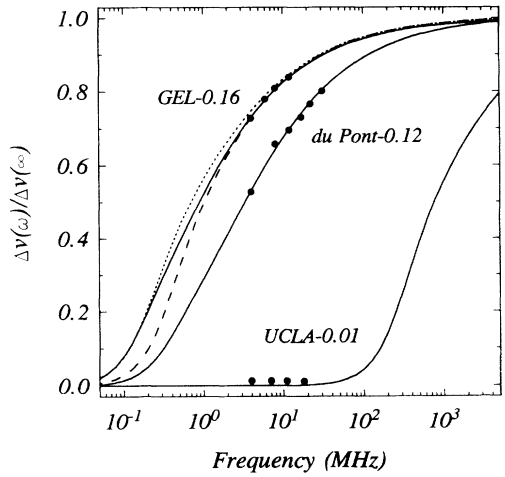

FIG. 16. The velocity crossover in the three samples. The velocity change with respect to low frequency, $\Delta v(\omega) = v(\omega) - v(0)$, is normalized by the total change from low to high frequency, $\Delta v(\infty) = v(\infty) - v(0)$. The symbols are the data at a temperature of 2.2 K (just above T_λ). The solid lines are the Biot predictions at the same temperature, calculated using the parameters from Table I. The dotted and dashed lines have the same meanings as in Fig. 15.

which are far enough in the high-frequency regime that up to about 80% of the helium is decoupled.

In Figs. 15 and 16 we also show the results of the two different calculations for the GEL-0.16 sample. The dashed lines are the Biot calculations using the independently measured permeability $\kappa_0 = 3.6 \times 10^{-11}$ cm^2 rather than the "best-fit" value $\kappa_a = 6 \times 10^{-11}$ cm^2. In the experimental frequency range the results are almost indistinguishable, showing that measurements in the low-frequency range are needed to determine the permeability with any accuracy. The dotted lines were calculated using the same parameters as for the solid lines, but using the simplified form suggested by Johnson, Koplik, and Dashen[10] for $F(\omega)$. As they pointed out, their function differs little from the more complicated cylindrical pore expression (7) and any smooth interpolation between the low- and high-frequency regimes would probably be adequate to determine κ_a and Λ. From Figs. 15 and 16, it is clear that measurements over a much wider frequency range are required if we are to draw conclusions about distributions of pore sizes and broadening of the crossover region beyond that of the Biot model. The measurements we described in our earlier paper were made on a sample similar to du Pont–0.12, so Gist was correct in suggesting that the Biot model could still describe our results if the effective pore size was considerably smaller than 1 μm.

We have demonstrated that measurements of the velocity and attenuation of shear waves may be used to determine the parameters which characterize the geometry of a porous medium. Measurements at ultrasonic frequencies are suitable for materials with submicrometer pores, while slow-wave measurements (especially fourth and second sound in superfluid helium) are more useful for larger pores. Despite the irregular pore structure of the samples (ceramics made either by sintering alumina powders or by a sol-gel process), the Biot model provided a good quantitative fit to the velocity and attenuation over the complete temperature and frequency range of the measurements. Since the permeabilities of the samples varied by more than three orders of magnitude, we were able to make measurements in both the low-frequency (UCLA-0.01 sample) and the high-frequency (du Pont–0.12 and GEL-0.16 samples) regimes. From the attenuation measurements in the UCLA-0.01 sample we found a permeability which was within a factor of 2 of that measured in a static flow measurement. For the other two samples we were able to determine the size parameter Λ. Table I shows the geometrical parameters determined for the three samples. It is clear that the combination $M = 8c\kappa_0/\phi\Lambda^2$ is close to 1, as suggested by Johnson and co-workers. Since this appears to hold in porous media with very different structures it may allow the permeability to be predicted from acoustic measurements (of either slow or fast modes) at high frequency. Note particularly that the value $M = 1.47$ for the sample with 92% porosity is about an order of magnitude larger than that calculated for similar porosities in the models of Chapman and Higdon.[12] However, the solid matrix in our sample, although tenuous, is still completely connected and rigid, in contrast to the isolated spheres of their model in the high-porosity limit. It appears that M is close to 1 even in materials with very open geometries where realistic models of porous media have not yet been studied.

ACKNOWLEDGMENTS

Acknowledgment is made to the Donors of the Petroleum Research Fund, administered by The American Chemical Society, for the support of this research. This work was also supported in part by a grant from the Natural Sciences and Engineering Research Council of Canada. We would like to thank Gary Williams and Kevin Ewsuk for providing samples.

*Present address: Daniel Industries, Houston, TX.

[1]B. R. Tittman,, J. R. Bulau, and M. Abdel-Gawad, in *Physics and Chemistry of Porous Media,* edited by D. L. Johnson and P. N. Sen (AIP, New York, 1984).

[2]J. Dvorkin and A. Nur, Geophysics **58**, 524 (1993); J. Dvorkin, R. Nolen-Hoeksema, and A. Nur, *ibid.* **59**, 428 (1994).

[3]T. D. Jones, Geophysics **51**, 1939 (1986).

[4]W. F. Murphy, K. W. Winkler, and R. L. Kleinberg, Geophysics **51**, 757 (1986).

[5]M. A. Biot, J. Acoust. Soc. Am. **28**, 168 (1956); **28**, 179 (1956).

[6]D. L. Johnson, T. J. Plona, and H. Kojima, in *Physics and Chemistry of Porous Media,* edited by J. Banavar, J. Koplik, and K. Winkler (AIP, New York, 1987); D. L. Johnson, D. L. Hemmick, and H. Kojima, J. Appl. Phys. **76**, 104 (1994); D. L. Johnson, T. J. Plona, and H. Kojima, *ibid.* **76**, 115 (1994).

[7]K. L. Warner and J. R. Beamish, Phys. Rev. B **36**, 5698 (1987); **39**, 7298 (1989).

[8]G. A. Gist, Phys. Rev. B **39**, 7295 (1989).

[9]D. L. Johnson, J. Koplik, and L. M. Schwartz, Phys. Rev. Lett. **57**, 2654 (1986).

[10]D. L. Johnson, J. Koplik, and R. Dashen, J. Fluid Mech. **176**, 379 (1987).

[11]M.-Y. Zhou and P. Sheng, Phys. Rev. B **39**, 12 027 (1989); P. Sheng, M.-Y. Zhou, E. Charlaix, A. P. Kushnick, and J. P. Stokes, Phys. Rev. Lett. **63**, 581 (1989).

[12]A. M. Chapman and J. J. L. Higdon, Phys. Fluids A **4**, 2099 (1992).

[13]L. M. Schwartz, N. Martys, D. P. Bentz, E. J. Garboczi, and S. Torquato, Phys. Rev. E **48**, 4584 (1993).

[14]Y. Achdou and M. Avellaneda, Phys. Fluids A **4**, 2651 (1992).

[15]R. B. Saeger, L. E. Scriven, and H. T. Davis, Phys. Rev. A **44**, 5087 (1991).

[16]E. Charlaix, A. P. Kushnick, and J. P. Stokes, Phys. Rev. Lett. **61**, 1595 (1988).

[17]D. M. J. Smeulders, R. L. G. M. Eggels, and M. E. H. van Dongen, J. Fluid Mech. **245**, 211 (1992).

[18]D. L. Johnson, Phys. Rev. Lett. **63**, 580 (1989).

[19]S. R. Pride, F. D. Morgan, and A. F. Gangi, Phys. Rev. B **47**, 4964 (1993).

[20]D. K. Wilson, J. Acoust. Soc. Am. **94**, 1136 (1993).

[21]D. L. Koch, Phys. Fluids **20**, 2922 (1987).
[22]T. J. Plona, Appl. Phys. Lett. **36**, 259 (1981).
[23]D. L. Johnson, Appl. Phys. Lett. **37**, 1065 (1980).
[24]D. L. Johnson, in *Frontiers of Physical Acoustics,* Proceedings of the International School of Physics "Enrico Fermi," Course LXXXXIII, Varenna on Lake Como, 1984, edited by D. Sette (North-Holland, Amsterdam, 1986).
[25]For a review of the properties of superfluid helium, see, for example, S. Putterman, *Superfluid Hydrodynamics* (North-Holland, Amsterdam, 1974).
[26]M. J. Lea, P. Fozooni, and P. W. Retz, J. Low Temp. Phys. **54**, 303 (1984).
[27]D. Singer, F. Pasierb, and H. Kojima, Phys. Rev. B **30**, 2909 (1984).
[28]S. R. Baker, Ph.D. thesis, University of California, Los Angeles, 1986.
[29]D. Salin and W. Schon, J. Phys. (Paris) Lett. **22**, L477 (1981).
[30]J. M. Hovem and G. D. Ingram, J. Acoust. Soc. Am. **66**, 1807 (1979).
[31]J. R. Beamish, A. Hikata, and C. Elbaum, Phys. Rev. B **27**, 5848 (1983); J. R. Beamish and N. Mulders, in *Quantum Fluids and Solids,* edited by G. G. Ihas and Y. Takano (AIP, New York, 1989).
[32]D. Tingzhang, I. Iwasa, and A. J. Ikushima (unpublished).
[33]S. Brunauer, P. H. Emmett, and E. Teller, J. Am. Chem. Soc. **60**, 309 (1938).
[34]M. Bernard and G. A. Williams, Phys. Rev. Lett. **67**, 2585 (1991); M. Bernard, Ph.D. thesis, University of California, Los Angeles, 1992.
[35]This sample was prepared by K. Ewsuk, E. I. du Pont de Nemours and Co., Wilmington, Delaware.
[36]D. McQueeney, G. Agnolet, and J. D. Reppy, Phys. Rev. Lett. **58**, 1325 (1984).
[37]For a recent review, see M. H. W. Chan, Physica B **169**, 135 (1991).
[38]J. G. Berryman, Appl. Phys. Lett. **49**, 552 (1986).